63rd International Astronautical Congress 2012, Naples, Italy

IAC-12, C1, 6, 9, x14982

FAST NUMERICAL COMPUTATION OF LISSAJOUS AND QUASI-HALO LIBRATION POINT TRAJECTORIES AND THEIR INVARIANT MANIFOLDS

Josep–Maria Mondelo
IEEC & Universitat Autònoma de Barcelona, Spain, jmm@mat.uab.cat

Esther Barrabés
Universitat de Girona, Spain, barrabes@ima.udg.es

Gerard Gómez
IEEC & Universitat de Barcelona, Spain, gerard@maia.ub.es

Mercè Ollé
Universitat Politècnica de Catalunya, Spain, merce.olle@upc.edu

Abstract

In this paper we present a methodology for the automatic generation of quasi–periodic libration point trajectories (Lissajous and quasi–halo) of the Spatial, Circular Restricted Three–Body Problem. This methodology is based on the computation of a mesh of orbits which, using interpolation strategies, gives an accurate quantitative representation of the full set of libration point orbits. This representation, when combined with the one obtained using Poincaré maps, provides a useful tool for the design of missions to libration points fulfilling specific requirements. The same methodology applies to stable and unstable manifolds as well. This paper extends and improves results presented in [10].

I INTRODUCTION

Libration point orbits (LPO) have unique characteristics suitable for different kinds of spacecraft missions. Among their most relevant characteristics, one can mention:

(a) In the Earth–Sun system, they are easy and inexpensive to reach from Earth [4].

(b) In the Earth–Sun system, they provide good observation sites, mainly solar observatories at L_1 and astronomy observatories at L_2. Near L_2 more than half of the entire celestial sphere is available at all times.

(c) Since the libration orbits around the L_1 and L_2 points of the Sun–Earth system always remain close to the Earth, at a distance of roughly 1.5 million km, and have a near-constant geometry as seen from the Earth, the communications system is simple.

(d) The L_2 environment of the Sun–Earth system is highly favourable for non-cryogenic missions requiring great thermal stability, suitable for highly precise visible light telescopes.

(e) The libration orbits around the L_2 point of the Earth–Moon system can be used to establish a permanent communications link between the Earth and the hidden part of the Moon, as was suggested by A.C. Clark in 1950 [3].

(f) LPO can provide ballistic planetary captures, such as for the one used by the Hiten spacecraft [8].

(g) Heteroclinic connections between LPO provide Earth transfer and return trajectories, such as the one used for the Genesis mission [9] or by the Artemis-P1 spacecraft.

(h) LPO provide interplanetary transport which can be exploited in the Jovian and Saturn systems to design a low energy cost mission to tour several of their moons (Petit Grand Tour mission) [5].

(i) Formation flight, with a rigid shape, is possible using LPO [1].

The unstable character of LPO provides them with stable and unstable manifolds, that enable transfers from the small primary (as in (a) above), heteroclinic transfers (as in (g)) or transfers inside the same family [4].

Within the last twenty years new analytical tools have been developed that provide approximations for many different solutions around the libration points in a number of dynamical models, and that include various types of periodic and quasi-periodic motions in their vicinity. The structure of the phase space in the vicinity of the collinear points has been studied and the fundamental motions determined, including the periodic halo orbits, as well as Lissajous trajectories and quasi-halos. The capability to numerically and analytically produce these types of motion, for different dynamical models, in a fast and efficient way is an ongoing development. The local behaviour near these orbits is also of critical importance in any effort to develop general methodologies for mission analysis and has been the focus of several studies. These studies have been directly responsible for the application of invariant manifolds to ultimate produce viable nominal and transfer trajectories for several missions.

Unique to upcoming missions are the designs of constrained transfer trajectories and mission orbits. They are designed to meet orbit goals for small Lissajous orbits, to minimise fuel and operational requirements and to provide formation or constellation options. Traditionally, libration orbit design has been analysed with a baseline trajectory concept set in place by project requirements or analytical boundary methods. That is, a trajectory had been base-lined so that science requirements are met. Future mission design requires a more generalised approach as operational considerations require the launch window, gravity assist, transfer trajectories, final orbits and the number of spacecraft to be as flexible as possible to optimise science return while minimising operational and launch requirements.

As a consequence, and in order to satisfy the increasingly demanding requirements of libration point missions, it is desirable to have parametric descriptions of the trajectories around the libration points, together with their associated invariant manifolds, as global as possible. Moreover, trajectories for specific values of the parameters should be retrieved in a fast and simple way. We think that this will make easier and faster the choice of the suitable nominal and transfer trajectories for the mission designer. The development of methodology to fulfil these objectives is the main goal of the present paper.

The linear character of the flow around the collinear libration points of the Restricted Three Body Problem is centre $\times$ centre $\times$ saddle, so they have a 4–dimensional centre manifold in which lie all the nominal trajectories interesting for libration point missions. This centre manifold has 5–dimensional stable and unstable manifolds, made by the stable and unstable manifolds of its individual trajectories, which fill large neighbourhoods of the libration points in 6–dimensional space.

From these considerations follows that, when dealing with libration point orbits, we have to face with objects inside a high dimensional space, very difficult to be represented, wherein a four dimensional set of libration point orbits act as saddle points. To overcome the technical difficulties due to these facts, several mathematical tools have been developed up to present, and are essentially based in normal forms or in Lindstedt-Poincaré procedures. They pretend, in some way, to decrease the number of degrees of freedom as well as to decouple the hyperbolic parts from the elliptical ones, in order to simplify and study the problem from a mathematical point of view. They are one of the bases for the construction of new devices that permit mission analysis in a systematic way, avoiding trial and error strategies as much as possible.

Both methodologies, normal form and Lindstedt-Poincaré procedures, provide full descriptions of the

orbits in selected energy levels. Nevertheless, they have several weak points. For instance, the energy level must be close to the one of the libration point, some of the variables used for the description of the flow do not have any physical meaning, the evaluation of the expansions can be time consuming, the change of variables from the usual position and velocity to amplitudes and phases must be implemented through iterative numerical procedures, etc.

Some of the drawbacks of the two above mentioned methodologies can be overcome by using numerical techniques for the computation of the families of periodic orbits and invariant tori of the centre manifold, as well as their invariant manifolds. The methodology for the computation of periodic orbits and their invariant manifolds is a classical one in simulation of dynamical systems. The computation of tori and their invariant manifolds is more recent and allows to obtain new families of invariant tori, apart from the well-known Lissajous orbits and quasi–halo orbits. Numerical techniques have a drawback on its own, which is that they produce individual trajectories but not parametrisations of families of trajectories.

The combination of the best properties of each methodology, with an effective implementation of the numerical procedures, is the basis for obtaining very efficient gadgets for mission design in the Solar System using libration points. A snapshot of a prototype of such a gadget, developed by our group in Barcelona, is shown in Fig. 1. This gadget is now based exclusively on a Poincaré map representation (Section II.II) and allows to chose trajectories and manifolds of a single energy level. The use of an energy–rotation number representation (Section II.I) would allow to browse trajectories of several energies.

The goal of this paper is to show how to get in a fast and easy way the full set of orbits in a large energy range, together with their invariant stable and unstable manifolds, using an interpolation procedure over a sufficiently fine mesh of orbits. After this introduction, Section II introduces the necessary representations of libration point trajectories in order to give in Section III the details of the computation of the meshes, interpolation and some characteristics of the families of trajectories described. Finally, Section IV provides an overview of the numerical methodology used in all the computations presented.

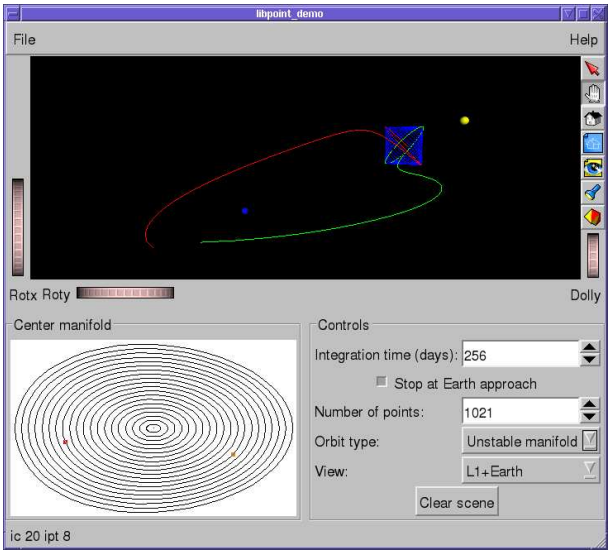

Fig. 1: Snapshot of a prototype of a possible gadget for the design of libration point trajectories.

With respect to reference [10], we have added the quasi–halo family and improved the interpolation procedure using finite elements.

II REPRESENTATION OF LIBRATION POINT ORBITS

The reference model that will be used is the circular restricted three body problem (CRTBP). As it is well known [11], this problem studies the behaviour of a particle with infinitesimal mass moving under the gravitational attraction of two primaries revolving around their centre of masses in circular orbits.

Using a suitable reference system and a dimensionless set of units, the equations of motion can be written as

$$\begin{aligned} \ddot{x} - 2\dot{y} &= x - \frac{(1-\mu)}{r_1^3}(x-\mu) - \frac{\mu}{r_2^3}(x+1-\mu), \\ \ddot{y} + 2\dot{x} &= y - \frac{(1-\mu)}{r_1^3}y - \frac{\mu}{r_2^3}y, \\ \ddot{z} &= -\frac{(1-\mu)}{r_1^3}z - \frac{\mu}{r_2^3}z, \end{aligned} \tag{1}$$

where $\mu = m_2/(m_1+m_2)$, being m_1, m_2 the masses of the primaries with $m_1 > m_2 > 0$, and $r_1 = [(x-\mu)^2 + y^2 + z^2]^{\frac{1}{2}}$, $r_2 = [(x+1-\mu)^2 + y^2 + z^2]^{\frac{1}{2}}$

are the distances from the infinitesimal mass particle to the two primaries.

By introducing momenta as $p_x = \dot{x} - y$, $p_y = \dot{y} + x$ and $p_z = \dot{z}$, the equations of the CRTBP can be written in hamiltonian form with Hamiltonian function

$$H = \frac{1}{2}(p_x^2 + p_y^2 + p_z^2) - xp_y + yp_x - \frac{1-\mu}{r_1} - \frac{\mu}{r_2}.$$

The Hamiltonian is related to the well known Jacobi first integral through

$$C = -2H + \mu(1-\mu).$$

The above CRTBP equations have five equilibrium points, the so called libration points. Three of them, the collinear libration points, are in the line joining the primaries and they are usually denoted as L_1, L_2 and L_3. The other two are the triangular ones, and are in the plane of motion of the primaries forming an equilateral triangle with them. If x_{L_i} $(i = 1, 2, 3)$ denotes the abscissa of the three collinear points, we will assume that

$$x_{L_2} < \mu - 1 < x_{L_1} < \mu < x_{L_3},$$

and we will focus our attention in L_1.

The motion in the vicinity of the collinear equilibrium points can be seen as the composition of two oscillators and some "hyperbolic" behaviour. This means that the oscillations are not stable and that very small deviations will be amplified as time increases. One of the oscillations takes place in the plane of motion of the primaries and the other orthogonal to this plane. These two periodic motions are known as the planar and vertical Lyapunov periodic orbits. The frequencies of the oscillations vary with the amplitudes (since the problem is not linear), and for a suitable amplitude both frequencies become equal. At this point the well known halo–type periodic orbits appear. When the frequencies of the two oscillations (vertical and planar) are not commensurable, the motion is not periodic and it reminds a Lissajous orbit. Then we say that we have a quasi-periodic orbit. This kind of motion can be found both around the vertical periodic orbit and around the halo orbits.

A more synthetic way of displaying all this zoo of orbits consists in representing only their intersection with the $z = 0$ plane. This is what is usually called a Poincaré map representation. A planar orbit will appear as a closed curve on the plane and a quasi-periodic orbit as a set of points lying, more or less, on a smooth closed curve. Fig. 2 shows one of these representations. Near the centre of the figure one can see a fixed point. It corresponds to a vertical periodic orbit that crosses the $z = 0$ plane just at this point. It (and so, the corresponding orbit) is surrounded by quasi-periodic motions that take place on invariant tori. The external curve of the figure is the planar Lyapunov orbit (corresponding to a given value of the Jacobi constant). The two other fixed points are associated to the two halo orbits, which are symmetrical to one another with respect to $z = 0$. They are, in turn, surrounded by invariant 2D tori. Between the 2D tori around the vertical orbit and the ones around the halo orbit there is the trace of the stable and unstable manifolds of the planar Lyapunov orbit, which acts as a separatrix between two different kinds of motion: the ones around the vertical periodic orbits and the ones around the halo orbits.

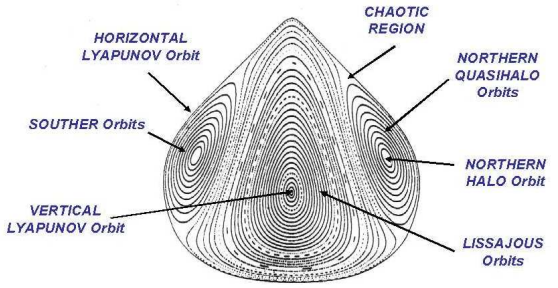

Fig. 2: Poincaré map representation of the orbits near the libration point L_1 for the value of the Jacobi constant 3.00078515837634. The CRTBP mass parameter corresponds to the Earth+Moon–Sun system. The coordinates in this representation are not physical, but correspond to the normal form reduction mentioned in the text.

Due to the unstable behaviour of the collinear libration points, this Poincaré map representation cannot be obtained by direct numerical integration of the CRTBP equations of motion. Fig. 2 was obtained after performing a normal form reduction of the Hamiltonian of the CRTBP and removing from the reduced Hamiltonian its unstable terms. Of course, this 2-dimensional figure corresponds to a fixed energy level (fixed value of the Jacobi constant or, equivalently, of the Hamiltonian). To get a global represen-

tation of the 4-dimensional central manifold around the libration point (recall that for the representation we have fixed the value of the z-coordinate equal to zero, which reduces in one unit the total dimension) we need to vary the value of the energy and for each energy level get the associated Poincaré map representation of the flow. This 3-dimensional picture can also be obtained by a more direct method. For this purpose we must compute the periodic orbits and invariant 2D tori of the centre manifolds of the libration points, using either Lindstedt-Poincaré or purely numerical procedures, and once they have been determined, represent their intersections with the $z = 0$ section for each energy level. To avoid the convergence problems of the Lindstedt-Poincaré method, we have selected the numerical procedures described in Section IV.

II.I Energy–rotation number representation of libration point orbits

The families of periodic orbits usually considered in the libration point regime (planar Lyapunov, vertical Lyapunov, halo) have normal behaviour with an elliptic component, that gives rise to families of 2D invariant tori surrounding them. The normal behaviour around a periodic orbit is determined by the eigenvalues of its monodromy matrix. Namely, consider $\boldsymbol{x}_0 \in \mathbb{R}^6$ an initial condition of a p.o. with period T_p, and denote by $\boldsymbol{\phi}_t$ the time–t flow of the CRTBP equations (Eq. 1). Since these equations are Hamiltonian, the monodromy matrix of the p.o., $D\boldsymbol{\phi}_{T_p}(\boldsymbol{x}_0)$, is symplectic. Its eigenvalues, denoted as Spec, are structured as

$$\mathrm{Spec}\, D\boldsymbol{\phi}_{T_p}(\boldsymbol{x}_0) = \{1, 1, \lambda_1, 1/\lambda_1, \lambda_2, 1/\lambda_2\}.$$

A pair of inverse eigenvalues $\lambda_i, \lambda_i^{-1}$ is said to be of:

- hyperbolic type, if $\lambda_i \in \mathbb{R}$, $\lambda_i \neq \pm 1$,
- elliptic type, if $\lambda_j = e^{i\nu}$ for $\nu \in (0, \pi)$,
- complex saddle, if $\lambda_j \notin \mathbb{R}$.

In the elliptic case, if we denote by $\boldsymbol{v}_0 + i\boldsymbol{v}_1$ an eigenvector of $D\boldsymbol{\phi}_{T_p}(\boldsymbol{x}_0)$ of eigenvalue $e^{i\nu}$ and define

$$\overline{\boldsymbol{\varphi}}(\xi) = \boldsymbol{x}_0 + \gamma\big(\boldsymbol{v}_1 \cos\xi + \boldsymbol{v}_2 \sin\xi\big),$$

for $\gamma > 0$, the propagation of the curve $\{\overline{\boldsymbol{\varphi}}(\xi)\}_{\xi\in[0,2\pi]}$ through the linear flow gives an invariant torus around the p.o. with *rotation number* ν, meaning that the phase ξ advances ν radians in every revolution around the p.o. (see Fig. 3). This is due to the equality

$$\boldsymbol{\phi}_{T_p}\big(\overline{\boldsymbol{\varphi}}(\xi)\big) = \overline{\boldsymbol{\varphi}}(\xi + \nu) + O(\gamma^2),$$

that is obtained by a short calculation involving a first-order Taylor expansion of $\boldsymbol{\phi}_{T_p}$ around $\boldsymbol{x}_0$ and the use of the eigenvector–eigenvalue condition.

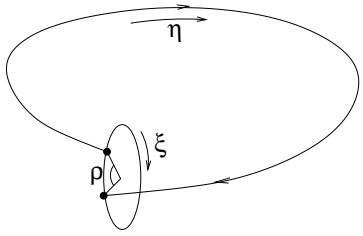

Fig. 3: Qualitative representation of the rotation number ρ.

For γ small, $\overline{\boldsymbol{\varphi}}(\xi)$ will be an approximation of an invariant curve of the full non–linear flow (this is, the flow of the CRTBP equations of Eq. 1). The methods sketched in Section IV.I and fully developed in [6] allow to turn it into a parametrisation $\boldsymbol{\varphi}(\xi)$ of a true invariant curve of the non–linear flow (up to a prescribed tolerance), satisfying the equation

$$\boldsymbol{\phi}_T\big(\boldsymbol{\varphi}(\xi)\big) = \boldsymbol{\varphi}(\xi + \rho).$$

Close to the periodic orbit, $T \approx T_p$ and $\rho \approx \nu$. As the invariant curve moves away from the p.o., both T and ρ vary. This makes the rotation number ρ a convenient parameter to identify a torus, together with its energy, that can be computed for instance as $h = H(\boldsymbol{\varphi}(0))$.

The previous considerations give rise to the *energy–rotation number* representation of families of invariant tori around a family of periodic orbits with elliptic normal behaviour. An example of such a representation is given in Fig. 4 for the quasi–halo trajectories around the L_1 point corresponding to the Earth–Moon mass parameter. In this figure, the points in the red curve represent the halo family of p.o., with $h = H(\boldsymbol{x}_0)$ and $\rho = \nu$ being $e^{i\nu}$ an eigenvalue of the monodromy matrix. Each point in the region delimited by the previous curve, the horizontal axis and the green curve corresponds to an invariant torus. The

green curve enclosing the region is not a dynamical boundary but computational one, and corresponds to the highest energies reached by continuation of invariant tori starting from the halo periodic orbits.[1] Actually, for the interpolation strategy described in section III, we have computed a grid of 73939 invariant tori, with a regular spacing of 0.0005 for energy and 0.0025 for rotation number.

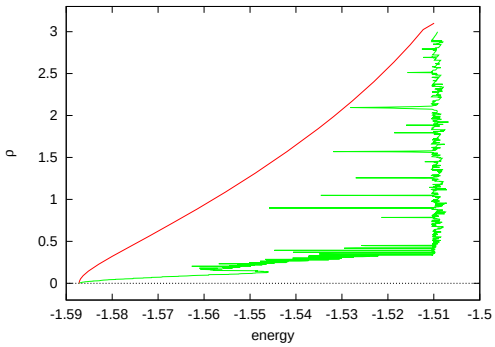

Fig. 4: Energy–rotation number representation of the quasi–halo family of invariant tori corresponding of the L_1 point of the Earth–Moon mass parameter of the CRTBP.

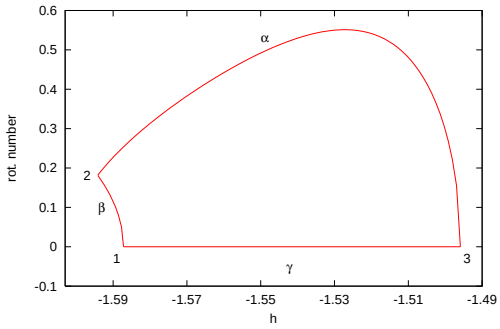

Fig. 5: Synthetic representation of the 2-parametric family of Lissajous orbits around the L_1 point, using as parameters the value of the Hamiltonian h and the rotation number ρ.

Fig. 5 displays the energy-rotation number representation of the two-parametric family of tori born from the vertical and planar Lyapunov families of periodic orbits (Lissajous orbits). Unlike in the previous case, the boundary of the region in the (h, ρ) covered by the computed tori is dynamical, and encloses the whole family. This boundary is made by three different curves:

- The upper piece α (from vertex 2 to 3) is related to the vertical Lyapunov family of periodic orbits in the same way the red curve of Fig. 4 is related to the halo family.
- The lower-left curve β (from vertex 1 to 2) is related to the planar Lyapunov family of periodic orbits. The orbits of this family represented in the curve are only those with an elliptic normal component, which are the only ones surrounded by tori. They are the "first" orbits of the family generated from the libration point. Each point (h, ρ) of this curve is related to the corresponding orbit in the planar family through the relations

$$h = H(\boldsymbol{x}_0), \quad \rho = \frac{(2\pi)^2}{2\pi - \nu} - 2\pi,$$

  assuming that $\boldsymbol{x}_0$ is an initial condition of the p.o. and $e^{i\nu}$ is an eigenvalue of its monodromy matrix. This difference with respect to points in the α curve is due to the fact that an invariant curve computed starting from a vertical p.o. approaches the planar family not as an invariant curve around a planar p.o. but as a planar p.o. itself. Full details can be found in [6].
- The bottom boundary γ (from vertex 3 to 1) that corresponds to $\rho = 0$, begins at the value of the energy where the halo families are born. It is related to a separatrix between the tori around the vertical Lyapunov families and the halo ones.

II.II Relation with the Poincaré map representation

Next, we can see how this synthetic representation of the 2-parameter family of Lissajous orbits is related to their Poincaré map representation at different energy levels. This is shown in Fig. 6. If in the (h, ρ) diagrams we fix a value of the energy and get a vertical segment connecting the β curve with the α or γ curve (depending on the value of h). For values of h lower than the one associated to the bifurcation of the halo families of periodic orbits (for instance, $h = -1.59$), the vertical segment connects β and α, which are associated, respectively, to the vertical and planar Lyapunov families of periodic orbits. This means that there is a 1-parameter family of Lissajous orbits (tori) connecting these two periodic orbits. The intersection of these Lissajous orbits with the $z = 0$

[1] The true extent of this family of tori is an open question

plane is displayed in the Poincaré map representation as a set of "concentric circles" with centre at the fixed point associated to the vertical periodic orbit and having as outer boundary the planar Lyapunov orbit. For any other value of h the vertical segment in the (h, ρ) goes from the β curve, associated to the vertical Lyapunov family, to the γ curve, for which $\rho = 0$. As it has been said, this last curve represents the separatrix between the tori around the vertical Lyapunov families and the halo ones, so now the 1-parameter family of Lissajous orbits will start also close to the vertical Lyapunov periodic orbit and will have a natural termination when it reaches the separatrix. The intersection of these Lissajous orbits with $z = 0$ are the closed magenta curves around the central fixed point in the Poincaré map representation. The red curves of the Poincaré map representation are traces of quasi-halo trajectories, that would give vertical lines in the h–ρ region of Fig. 4 corresponding to the energy levels shown in Fig.6.

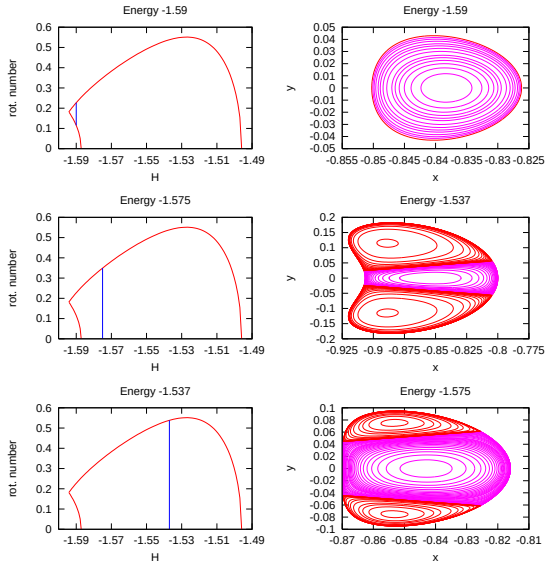

Fig. 6: Two synthetic representations of the 2-parametric family of Lissajous orbits around the L_1 point. In each (h, ρ) representation, the vertical (blue) line represents the family of Lissajous orbits around the vertical periodic orbit with a fixed value of the energy. In the Poincaré map representation, which is displayed below, these Lissajous orbits are represented by their intersection with $z = 0$ and are the closed curves in the centre of each plot coloured in magenta, around the central fixed point associated to the vertical periodic orbits. The red curves of the Poincaré maps are not related to the h–ρ diagrams of the first column, but correspond to the quasi–halo family represented in Fig. 4.

III FAST COMPUTATION OF LISSAJOUS AND QUASI–HALO TRAJECTORIES

The numerical methods outlined in section IV allow to compute individual trajectories. By applying continuation methods, one–parametric families of tori can be followed. For the case of tori around Lyapunov periodic orbits, any value of h, ρ in the diagrams previously shown can be reached by continuation, but this can be a rather time–consuming process. A fast way to obtain trajectories for any h, ρ is to interpolate between previously computed ones, provided they are part of a mesh fine enough for the interpolation to be accurate. This section is devoted to the presentation of results related to the implementation of this strategy.

A grid of invariant tori covering the (h, ρ) region of Lissajous orbits around L_1 for the Earth–Moon mass ratio (see Fig. 5) has been computed by numerical continuation with respect to h of several one–parametric families of tori with constant rotation number, starting from Lyapunov vertical and planar periodic orbits with energy smaller than the maximum of the curve β in Fig. 5. A total of 220 families have been continued, corresponding to an approximately uniform[2] spacing of ρ of 0.0025 units.

During the continuation of each family, Fourier series of tori have been stored for equally spaced values of h, with a spacing of 0.0005 units. The number of harmonics N_f has been increased as needed in order to obtain the error estimate of Eq. 6 smaller that 10^{-10} (3.85×10^{-5} km). The continuations have been stopped when the N_f has reached a maximum allowed value of 100 harmonics. The spacing in h and ρ used has been empirically determined in order to obtain an interpolation error of about 10^{-10} in most of the (h, ρ) region (see below). The computed grid of tori consists of a total of 25433 Fourier series of invariant curves, each one also with the error estimate of Eq. 6 smaller than 10^{-10}. The corresponding grids of invariant stable and unstable manifolds have been computed by solving the eigenvalue problem of Eq. 9 for each of the parametrisations φ of the grid of

[2] The rotation numbers have been "Diophantised" in order to be far from low–order resonances. See [6] for more details.

invariant tori.

In order to estimate the interpolation error on the region covered by the computed grids of tori and manifolds, the error estimates of Eqs. 6,10 have been evaluated on the Fourier series obtained by interpolation at the midpoints of the grids. The results are show in Figs. 7,8.

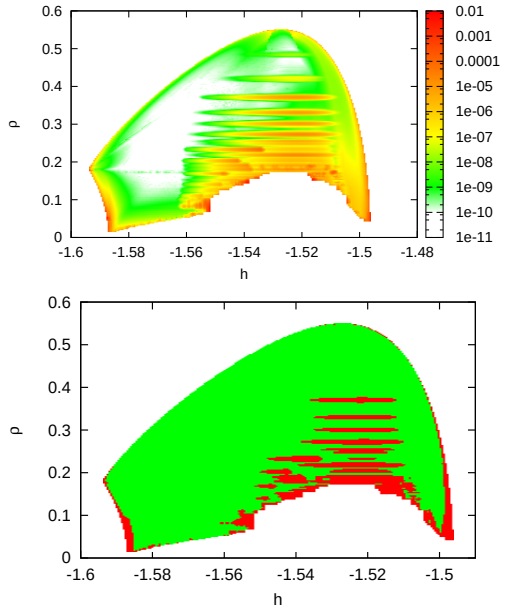

Fig. 7: Interpolation error on the midpoints of the grid of tori. Top: value of the estimate of Eq. 6. Bottom: interpolated tori with error estimate smaller than 10^{-6} (green), and larger than this value (red).

Fig. 7 shows that, in the case of tori, interpolation error ranges between 10^{-10} and 10^{-8} for most of the region. It increases in three different zones:

(a) Near the planar and vertical Lyapunov families of periodic orbits, this is, near the α and β curves of Fig. 5.

(b) In some horizontal strips, which correspond to resonances between the planar and vertical frequencies of the computed tori. From top to bottom, they correspond to the values $\rho = 2\pi/13, 2\pi/15, 2\pi/17, \ldots$

(c) Near the bottom of the region, this is, the γ curve of Fig. 5, which corresponds to the separatrix between quasi–periodic motions around Lyapunov vertical and halo periodic orbits.

In the (c) case it is natural to expect an increasing interpolation error, since it corresponds to the stopping of the continuation process during the computation of the grid, either by computational limit (reaching the maximum allowed value of N_f) or by breakdown of tori close to the separatrix.[3] For the (a) case, a refinement of the grid (recall that it is regularly spaced in h, ρ) is necessary in order to decrease the interpolation error. This can be done using finite elements, as discussed in Section III.I below. The reason for case (b) is dynamical. In solving Eq. 5 by continuation from lower energies, we are assuming that the Poincaré sections of the computed tori are closed curves like in the right column of Fig. 6, whereas the Poincaré sections of tori close to resonances are island chains. As an example, the the 1:17 resonance, corresponding to the $\rho = 2\pi/17$ strip in the top plot of Fig. 7, can be observed in Fig. 2 as an island chain. If high accuracy is needed, these resonant orbits should be computed as different families, as has been done in [6] for the quasi–halo case.

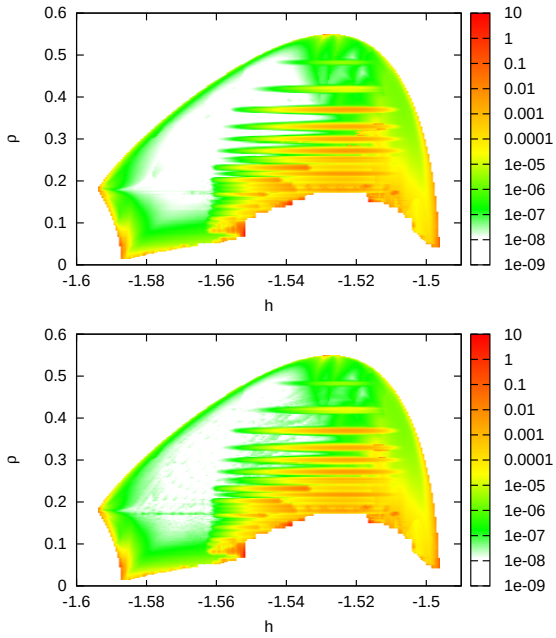

Fig. 8: Relative interpolation error on the midpoints of the grid of unstable (left) and stable (right) manifolds.

Fig. 8 shows the results corresponding to the evaluation of a relative error version of the estimate of

[3] This is a common phenomenon in Hamiltonian systems and is predicted by KAM theory.

Eq. 10,

$$\max_{\xi\in\mathbb{T}^1} \frac{\left\| D\phi_{T_2}\big(\varphi(\xi-\rho)\big)v(\xi-\rho) - \Lambda v(\xi)\right\|_2}{\|\Lambda v(\xi)\|_2},$$

on the midpoints of the grids of unstable and stable manifolds. It is seen that the error has the same qualitative behaviour as the error for tori shown in Fig. 7.

III.I Improving the interpolation using finite elements

An adaptive grid interpolation strategy can be designed with the use of finite elements (FE). This allows to benefit from all the literature on the application of FE to the solution of partial differential equations, see e.g. [2]. Given a triangle with vertices a_1, a_2, a_3 in (h, ρ) coordinates, closed-form formulae exist that allow the interpolation of a function $f(h, \rho)$ (a Fourier coefficient of an invariant curve, in our case) by a polynomial of degree n in two variables (h, ρ), computed from the values of f in points b_{n_1,n_2,n_3} regularly spaced in barycentric coordinates. This means that the points are of the form

$$b_{n_1,n_2,n_3} = \frac{n_1 a_1 + n_2 a_2 + n_3 a_3}{n}$$

with $0 \le n_1, n_2, n_3 \le n, \quad n_1 + n_2 + n_3 = n$. One of such formulae is [2]

$$p(\lambda_1 a_1 + \lambda_2 a_2 + \lambda_3 a_3) = \sum_{\substack{0\le n_1,n_2,n_3\le n \\ n_1+n_2+n_3=n}} f(b_{n_1,n_2,n_3})\psi_{n_1,n_2,n_3},$$

with $\lambda_1, \lambda_2, \lambda_3 \ge 0, \quad \lambda_1 + \lambda_2 + \lambda_3 = 1$, being

$$\psi_{n_1,n_2,n_3} = \frac{\prod_{j=1}^{3}\prod_{k=0}^{n_j-1}(n\lambda_j - k)}{\prod_{j=1}^{3} n_j!}$$

Fig. 9 shows an example of grid refinement using this strategy. The red crosses are nodes from the uniform grid of Fig. 7, in an (h, ρ) area where the interpolation error is of the order of 10^{-4}. The magenta square dots are nodes in (h, ρ) equally spaced on a triangle, with vertices on the family of planar Lyapunov p.o., for which the corresponding tori have been computed with error estimate under 10^{-10}. The red square dots are a further refinement of this triangle. A torus for any value of (h, ρ) in this last triangle recovered by fourth degree (two–dimensional) interpolation using the formulae above from the red square dots has an error estimate under 10^{-10}.

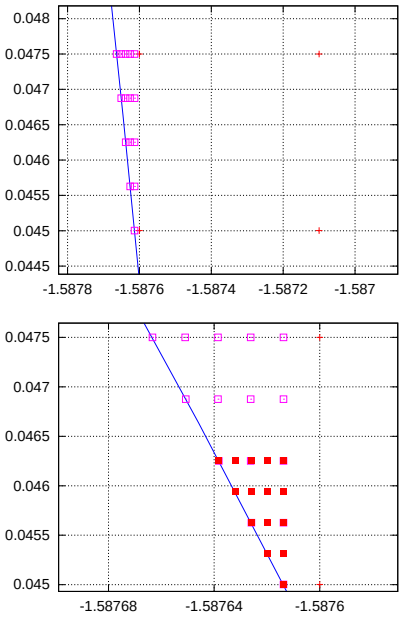

Fig. 9: Example of refinement of the uniform grid of Fig. 7 using finite elements.

III.II Metrics of the trajectories

In order to have an idea of the size of the orbits considered, Fig. 10 displays the behaviour of the size (in km) of the Lissajous invariant tori in terms of h, ρ. Only the midpoints of the grid of tori with interpolation error smaller than 10^{-6} (see Fig. 7 right) have been considered. For each torus, the maximum difference between the x, y, and z coordinates has been computed, by taking 128 equally spaced values of ξ and η in Eq. 7. It can be observed that, for constant ρ and increasing energies, the x and y amplitudes are non–monotonous, due to the fact that the corresponding one–parametric sub-families end at vertical Lyapunov periodic orbits (the β curve in Fig. 5), which have no planar amplitude. On the other hand, the z amplitude is always increasing with energy for constant ρ.

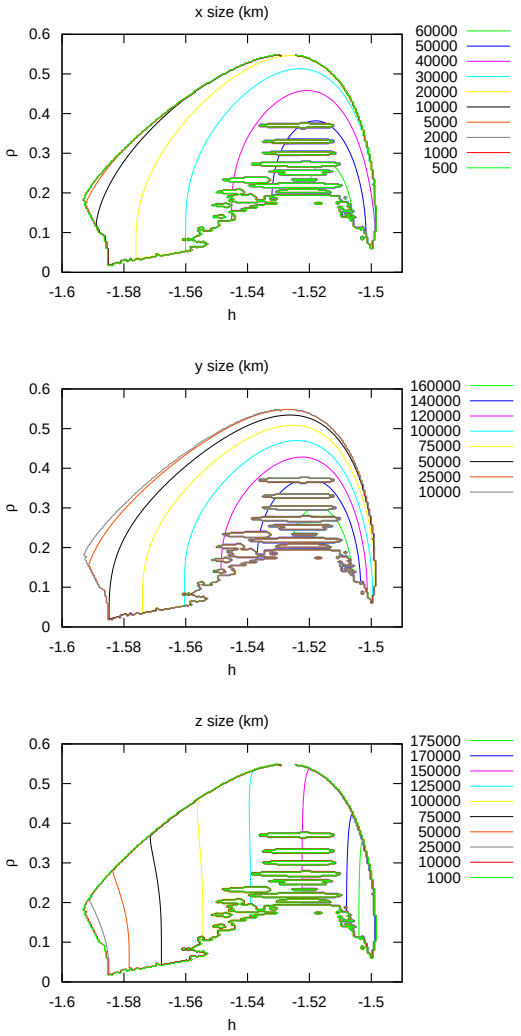

Fig. 10: Diagrams h–ρ displaying as level curves the size in the x, y and z coordinates the 2D tori of the Lissajous family around L_1 (for the Earth–Moon mass ratio). The units for size are km.

IV Numerical methodology

IV.I Numerical computation of invariant tori

Numerical methods have been widely used in the past to compute fixed points and periodic orbits. The computation of invariant tori is not so extended. The procedure that has been used is based in the computation of the Fourier series of an invariant curve on the torus [6]. This strategy is combined with a multiple shooting procedure in order to deal with the unstable behaviour of the flow.

Consider a 2-dimensional invariant torus of the CRTBP with frequencies $\omega = (\omega_1, \omega_2) \in \mathbb{R}^2$. If ϕ_t denotes the flow associated to the CRTBP, a parametrisation $\Psi : \mathbb{T}^2 = [0, 2\pi]^2 \to \mathbb{R}^6$ of the torus satisfies the following invariant relation:

$$\Psi \begin{pmatrix} \xi + \omega_1 t \\ \eta + \omega_2 t \end{pmatrix} = \phi_t \left(\Psi \begin{pmatrix} \xi \\ \eta \end{pmatrix} \right), \qquad (2)$$

for $\theta = (\xi, \eta) \in \mathbb{T}^2$ and $t \in \mathbb{R}$.

Let us denote by T_i the period corresponding to the ω_i frequency, that is $T_i = 2\pi/\omega_i$. In order to reduce dimensions, instead of considering a parametrisation of the whole torus, we can consider the parametrisation of a curve in the torus which is invariant under ϕ_{T_2}. Such a curve is given by $\{\eta = \eta_0\}$, since from Eq. 2 we have

$$\Psi \begin{pmatrix} \xi + \omega_1 T_2 \\ \eta_0 \end{pmatrix} = \phi_{T_2} \left(\Psi \begin{pmatrix} \xi \\ \eta_0 \end{pmatrix} \right),$$

for all $\xi \in \mathbb{T}^1$. If $\varphi : \mathbb{T}^1 \to \mathbb{R}^n$ is the parametrisation of this curve, then we require

$$\varphi(\xi + \omega_1 T_2) = \phi_{T_2}\big(\varphi(\xi)\big), \qquad (3)$$

for all $\xi \in \mathbb{T}^1$, where $\rho = \omega_1 T_2 = 2\pi\, \omega_1/\omega_2$ is the so called *rotation number* of the curve we are looking for. The rotation number ρ enables us to uniquely identify a torus at a given energy level, as it has been previously discussed.

It is convenient to assume for φ a truncated Fourier series representation

$$\varphi(\xi) = A_0 + \sum_{k=1}^{N_f} \big(A_k \cos(k\xi) + B_k \sin(k\xi) \big), \quad (4)$$

in which the unknowns A_k, $B_k \in \mathbb{R}^n$ depend on the value of the energy h (given by the value of the

Hamiltonian) and the rotation number ρ. Then, by taking $1 + 2N_f$ values of ξ, Eq. 3 can be turned into a finite–dimensional non–linear system of equations which can be solved for A_k, B_k. Concretely, we solve

$$\varphi(\xi_i + \rho) = \phi_{T_2}\big(\varphi(\xi_i)\big), \tag{5}$$

where $\xi_i = 2\pi/(1 + 2N_f)$ for $i = 0, \ldots, 2N_f$. The error due to the truncation of the Fourier series of φ can be estimated by evaluating the invariance equation (Eq. 3) in phases not used in the discretisation, that is, for $\xi \neq \xi_i$. Namely, the error estimate can be taken as

$$\max_{\xi\in\mathbb{T}^1} \big\| \varphi(\xi + \rho) - \phi_{T_2}\big(\varphi(\xi)\big) \big\|_2. \tag{6}$$

Once we have a parametrisation of an invariant curve, a parametrisation of the whole torus can be recovered by numerical integration, as

$$\Psi(\xi, \eta) = \phi_{\frac{\eta}{2\pi}T_2}\Big(\varphi\big(\xi - \frac{\eta}{2\pi}\rho\big)\Big). \tag{7}$$

The details of the computational aspects (non–uniqueness of the Fourier representation, dealing with instability, actual implementation, computing effort, parallel strategies, etc.) of this procedure are given in [6].

IV.II Numerical computation of invariant stable/unstable manifolds

The linear approximation of stable/unstable manifolds of periodic orbits can be numerically computed in a simple manner from the hyperbolic eigenvectors of the monodromy matrix. For invariant tori the situation, although similar, is not trivial. In our computations we have used the procedure introduced in [7]. The basic idea is the following: assume that $\xi \to \varphi(\xi)$ parametrises an invariant curve on a torus satisfying the invariant relation

$$\varphi(\xi + \omega_1 T_2) = \phi_{T_2}\big(\varphi(\xi)\big).$$

We look for a 2π–periodic function $v : \mathbb{R} \to \mathbb{R}^6$ giving the linear approximation of the stable/unstable manifold at $\varphi(\xi)$, this is

$$D\phi_{T_2}\big(\varphi(\xi)\big)v(\xi) = \Lambda v(\xi + \omega_1 T_2) = \Lambda v(\xi + \rho),$$

for a certain Λ which is called, analogously to the case of periodic orbits, characteristic multiplier. If $\Lambda > 1$ we obtain the unstable direction, and if $\Lambda < 1$ we obtain the stable one. To find solutions of the above equation, we first rewrite it as

$$D\phi_{T_2}\big(\varphi(\xi - \rho)\big)v(\xi - \rho) = \Lambda v(\xi). \tag{8}$$

The use of finite Fourier expansions allows to transform Eq. 8 into a finite–dimensional eigenvalue problem,

$$M\boldsymbol{c} = \Lambda\boldsymbol{c}, \tag{9}$$

where $\boldsymbol{c}$ is the vector of Fourier coefficients of $v(\xi)$, and M is a suitable (finite, but large) matrix. The error due to the truncation of the Fourier series of $v(\xi)$ again can be estimated using the invariance equation (Eq. 8). Namely, we can take as error estimate

$$\max_{\xi\in\mathbb{T}^1} \big\| D\phi_{T_2}\big(\varphi(\xi - \rho)\big)v(\xi - \rho) - \Lambda v(\xi) \big\|_2. \tag{10}$$

As discussed in [7], the eigenvalues of the discretised equation (Eq. 9) appear grouped in circles. If the torus is reducible, this is, the linear variational equations with quasi-periodic coefficients can be reduced to constant coefficients, then there are as many circles as eigenvalues of the reduced monodromy matrix and each circle contains one of them. In our case, due to the Hamiltonian character of the CRTBP, we have four unit circles and two additional circles containing Λ and Λ^{-1} for some $\Lambda > 1$. The associated eigenvectors $v_\Lambda(\xi)$ and $v_{\Lambda^{-1}}(\xi)$ give the linear approximation of the unstable/stable manifolds.

Once we have the linear approximation of the invariant manifolds associated to an invariant curve of the torus, we can globalise it using

$$v(\xi, \eta) = \Lambda^{-\eta/2\pi} D\phi_{\frac{\eta T_2}{2\pi}}\Big(\varphi\big(\xi - \frac{\eta}{2\pi}\rho\big)\Big)\, v\big(\xi - \frac{\eta}{2\pi}\rho\big).$$

In Fig. 11 we show the 3D unstable manifold associated to a Lissajous orbit around L_1 for different values of η when $\xi \in [0, 2\pi]$.

V CONCLUSIONS

In this paper, it has been shown how to apply numerical techniques to accurately compute libration point orbits (tori) and their stable and unstable manifolds. Two interpolation procedures have been designed, which allow to parametrically describe families of libration point orbits and their invariant manifolds in a

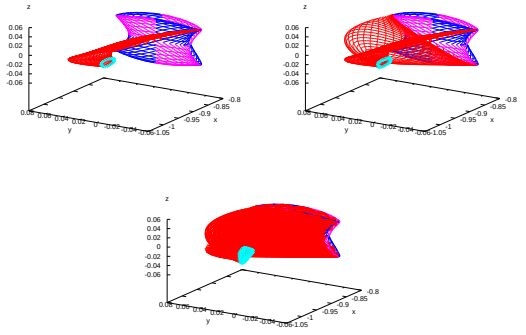

Fig. 11: Unstable manifold associated to a Lissajous orbit at: $\eta = 0$, $\eta = 0, \pi$ and at 15 different values of η equally spaced in $[0, 2\pi]$.

global way. These procedures have been illustrated for the L_1 point, Earth–Moon mass ratio, with the computation a fine grid of Lissajous and quasi–halo trajectories, as well as their corresponding invariant manifolds.

VI ACKNOWLEDGEMENTS

This work has been partially supported by the Spanish grants MTM2010-16425 (E.B., G.G., J.M.M.), MTM2011-26995-C02-01 (J.M.M.), MTM2009-06973 (M.O.), and the Catalan grants 2009-SGR-410 (J.M.M.), 2009-SGR859 (M.O.). The numerical explorations have been carried out in the Beowulf clusters Antz (Universitat Autònoma de Barcelona) and Hidra (Universitat de Barcelona).

References

[1] C. Beichman, G. Gomez, M. Lo, J. Masdemont, and L. Romans. Searching for life with the terrestrial planet finder: Lagrange point options for a formation flying interferometer. *Advances in Space Research*, 34:637–644, 2004.

[2] P. G. Ciarlet. *The finite element method for elliptic problems*. North-Holland Publishing Co., Amsterdam, 1978. Studies in Mathematics and its Applications, Vol. 4.

[3] R. Farquhar. The control and use of libration point satellites. Technical report, Stanford University, 1968. Report SUDAAR–350, reprinted as NASA TR R–346, 1970.

[4] G. Gómez, À. Jorba, C. Simó, and J. Masdemont. Study of the transfer between halo orbits. *Acta Astronautica*, 43(9–10):493–520, 1998.

[5] G. Gómez, W. S. Koon, M. W. Lo, J. E. Marsden, J. Masdemont, and S. D. Ross. Connecting orbits and invariant manifolds in the spatial restricted three-body problem. *Nonlinearity*, 17(5):1571–1606, 2004.

[6] G. Gómez and J. Mondelo. The Dynamics Around the Collinear Equilibrium Points of the RTBP. *Physica D*, 157(4):283–321, 2001.

[7] A. Jorba. Numerical computation of the normal behaviour of invariant curves of n–dimensional maps. *Nonlinearity*, 14:943–976, 2001.

[8] W. Koon, M. W. Lo, J. E. Marsden, and S. Ross. Low energy transfer to the moon. *Celestial Mechanics and Dynamical Astronomy*, 81(1–2):63–73, 2001.

[9] M. Lo, B. Williams, W. Bollman, D. Han, Y. Hahn, J. Bell, E. Hirst, R. Corwin, P. Hong, K. Howell, B. Barden, and R. Wilson. Genesis mission design. In AAS/AIAA Space Flight Mechanics, Paper No. AIAA 98–4468, 1998.

[10] J. M. Mondelo, E. Barrrabés, G. Gómez, and M. Ollé. Automatic generation of Lissajous–type Libration Point trajectories and its manifolds for large energies. Proceedings of the 21th International Sysmposium on Space Flight Dynamics, Toulouse (France) Sept. 28–Oct. 2, 2009.

[11] V. Szebehely. *Theory of Orbits*. Academic Press, 1967.